

Modelling the Magnetic Activity in the Sun and Sun-Like Stars

Visualization of the Magnetohydrodynamic Flow Inside the Convective Envelope with Meridional Circulation

C. Sağiroğlu¹

¹ Department of Physics Engineering, Graduate School of Science Engineering and Technology, Istanbul Technical University, 34469, Maslak, Istanbul, Turkey
e-mail: sagirogluc@itu.edu.tr

May 30, 2019

ABSTRACT

Context. To investigate the physical nature of the magnetohydrodynamic flow that influences the dynamo processes of the magnetic activity cycles in G-type-main-sequence stars like the Sun by producing graphical outputs of various meridional circulation profiles.

Aims. This study aims to show the difference between various meridional circulation profiles, their respective flow vectors and how they recycle throughout the convective interior of a G-type-main-sequence star, specifically the Sun. This proved to be an important aspect of modelling the magnetic activity cycle since the dynamo process relies heavily on the transportation of convective fluids inside the convective envelope.

Methods. I use Python 2.7.15 programming language to compute the meridional circulation profiles, their respective meridional flow vectors and produce their graphical output to lay the ground for an analysis of their radial and angular dependence and how they might effect the stellar dynamo.

Results. Hemispheric radial and angular distribution of meridional circulation behaviour is dictated by the exponent of the stratified convective zone m , amplitude for the surface and subsurface return flow p and amplitude of rising and sinking flow at lower and higher altitudes signifying the radial dependence q . Strength of the flow is dictated by the amplitude of the flow u_0

Conclusions.

Key words. Sun: activity — Sun: interior — Sun: magnetic fields — sunspots—Sun: Meridional Circulation

1. Introduction

Stellar magnetic activity in G-type-main-sequence stars has been an important area of study since the star of our solar system The Sun is a G2V spectral type-main-sequence star. Not only it has an influence on immeasurable amount of interaction within the solar system but it has a direct impact on Earth, atmospheric activity and satellites.(see Solanki et al. 2006)

Recent studies on solar magnetic activity point a tendency towards Mean Field Dynamos(MFD) (see Jouve et al. 2008) and Flux Transport Dynamos(FTD) (see Jiang et al. 2013; Schüssler & Schmitt 2004). Both of the models cherish poloidal to toroidal field shearing by differential rotation and take turbulent environmental effects, advective-diffusive transports and recycle action of the dynamo into consideration but their concentrations on how the process of toroidal flux ropes rise to the surface differentiate. Mean Field models tend to concentrate more on the dominance of turbulent effects and local kinematic helical contributions, while flux transport models concentrate mainly on the dominance of planetary rotation and its effects.

Starting with Babcock's suggestion (Babcock 1961) and elaboration of Leighton ((Leighton 1969)) and prececessors in coming years, concluded that bipolar solar spot regions that are formed in accordance with Joy's Law(Hale et al. 1919) and Hale's Law (Hale 1908), feed a magnetic network on the solar surface and polarity of the magnetic activity changes with 11

year periods. Models with such proposed behaviour are referred to as "Babcock-Leighton Dynamos".

The Babcock-Leighton process can be broken down into the following stages:

- Poloidal field considered at the bottom of the convection zone at the begining of a cycle, gets bended due to differential solar rotation,
- Shearing of the deep seated magnetic field produces a toroidal field antisymmetric about the equator,
- Buoyant magnetic flux tubes rise and pierce through the photosphere and produc sunspots. As a result of differential solar rotation they get bended towards the solar center and tilted accordingly, with respect to the direction of the toroidal flux in the given hemisphere,
- Sunspots go through latitudinal and longitudinal decay, spreading the flux in both directions throughout the cycle,
- Flux decay of oppositely polarized spots in each hemisphere, generate large scale meridional cell flow mechanism that carries the flux from the equator to the poles down to the bottom of the convection zone and back to the surface,
- Piling up of the flux to the poles eventually changes the sign of the poloidal field from the previous cycle and the dynamo recycles accordingly.

Large scale dynamo behaviour modelling the Babcock-Leighton model characterized by the Magneto Hydrodynamical

(MHD) Induction Equation can be written as

$$\frac{\partial \mathbf{B}}{\partial t} = \nabla \times (\mathbf{U} \times \mathbf{B} - \eta \nabla \times \mathbf{B}) \quad (1)$$

where \mathbf{B} is the magnetic field, \mathbf{U} is the total flow and η is the magnetic diffusivity. Under axisymmetric assumption the magnetic and flow fields can be written as

$$\mathbf{B}(r, \theta, t) = \nabla \times (A(r, \theta, t)\hat{e}_\phi) + B(r, \theta, t)\hat{e}_\phi \quad (2)$$

$$\mathbf{U} = \mathbf{u}(r, \theta) + r \sin \theta \Omega(r, \theta) \hat{e}_\phi \quad (3)$$

where $\nabla \times (A(r, \theta, t)\hat{e}_\phi)$ is the poloidal component of the magnetic field and $A\hat{e}_\phi$ is the poloidal potential, $B(r, \theta, t)\hat{e}_\phi$ is the toroidal component of the magnetic field, $\Omega(r, \theta)$ is the differential rotation and $\mathbf{u}(r, \theta)$ is the meridional circulation. Substitution of Eqs.2 and 3 into Eq.1 separates the poloidal and toroidal components of the governance of the dynamo action as can be seen from Eqs.3a, 3b in Dikpati & Charbonneau (1999).

2. Defining Meridional Circulation

Meridional circulation $\mathbf{u}(r, \theta)$ is a governing aspect of the total flow field \mathbf{U} and directly dictates the evolution of the poloidal and toroidal components of the magnetic field.

Angular components of the meridional circulation profiles u_θ from Dikpati & Charbonneau (1999) (noted as *profile1* from now on) and Dikpati et al. (2004) (noted as *profile2* from now on) are as follows

$$u_\theta(r, \theta) = u_o \left(\frac{R_\odot}{r} \right)^3 [-1 + c_1 \xi^m - c_2 \xi^{m+p}] \sin^{q+1} \theta \cos \theta \quad (4)$$

in which

$$c_1 = \frac{(2m+1)(m+p)}{(m+1)p} \xi_0^{-m} \quad (5)$$

$$c_2 = \frac{(2m+p+1)m}{(m+1)p} \xi_0^{-(m+p)} \quad (6)$$

$$\xi_0 = \frac{R_\odot}{r_b} - 1 \quad (7)$$

$$\xi(r) = \frac{R_\odot}{r} - 1 \quad (8)$$

where R_\odot is the radius of the Sun, $r_b = 0.7R_\odot$ radius at the bottom of the convective zone, m is the exponent of the stratified solar convective zone, p is the amplitude for the surface and subsurface return flow signifying the angular dependence, q is the amplitude of the rising sinking flow at lower and higher altitudes that signifying the radial dependence and u_o is the amplitude of the flow.

Radial components of the meridional circulation profiles u_r on the other hand, differ as

$$u_r(r, \theta) = u_o \left(\frac{R_\odot}{r} \right)^2 \times \left(-\frac{1}{m+1} + \frac{c_1}{2m+1} \xi^m - \frac{c_2}{2m+p+1} \xi^{m+p} \right) \times \xi \sin^q \theta [(q+2) \cos^2 \theta - \sin^2 \theta] \quad (9)$$

Table 1. The angular u_θ and radial u_r flow component, m, p and q used in each meridional circulation profile

Profile Number	u_θ	u_r	m	p	q
1 Dikpati & Charbonneau (1999)	4	9	0.50	0.25	0.00
2 Dikpati et al. (2004)	4	10	1.50	3.00	1.50

for *profile1*, and

$$u_r(r, \theta) = u_o \left(\frac{R_\odot}{r} \right) \times \left(-\frac{1}{m+1} + \frac{c_1}{2m+1} \xi^m - \frac{c_2}{2m+p+1} \xi^{m+p} \right) \times \xi \sin^q \theta [(q+2) \cos^2 \theta - \sin^2 \theta] \quad (10)$$

for *profile2*. Equations 4, 5, 6, 7 and 8 are same in both studies but they use different equations for u_r as demonstrated above and use different amplitudes m, p and q as shown in Table1.

3. Computation and Graphical Output

The code written in this study with Python 2.7.15 programming language, prompts the user for which of the meridional circulation profiles to be used between *profile1* and *profile2*, asks for a radial grid increment from a pool of choice containing $[0.01R_\odot, 0.02R_\odot, 0.05R_\odot, 0.1R_\odot]$, asks for an angular grid increment from a pool of choice containing $[1.0^\circ, 2.0^\circ, 3.0^\circ, 5.0^\circ, 10.0^\circ]$ and finally asks for flow amplitude u_0 in a range between $[1.0m.s^{-1}-200.0m.s^{-1}]$.

After taking the input from the user, the code computes u_r and u_θ with the given input references and values taken from Table1, produces two graphical outputs; one a quarter circle indicating the northern hemisphere of the Sun, the flow vectors, the flow field and the second being the radial variance of $u_\theta(r, \theta = 45^\circ)$ as presented on the preceding page from Fig. 1 through Fig. 8.

4. Results

It can be seen from Fig. 2 and Fig. 4 that the radial and angular distribution of the flow vectors vary with different meridional circulation profiles; in Fig. 2 the profile swarms around $0.86R_\odot$ whereas in Fig. 4 it does around $0.76R_\odot$ and in higher latitudes closer to the pole.

It can be seen from Fig. 1 and Fig. 3 that the radial behaviour of u_θ changes with different meridional circulation profiles; in Fig. 1 it reaches $0.5m.s^{-1}$ at $0.7R_\odot$, reaches a peak value of $1.0m.s^{-1}$ at $0.76R_\odot$ and reaches a minimum at $-10.0m.s^{-1}$ at $1.0R_\odot$ whereas in Fig. 3 it reaches $2.5m.s^{-1}$ at $0.7R_\odot$, reaches a peak value of $3.0m.s^{-1}$ at $0.76R_\odot$ and reaches a minimum at $-6.2m.s^{-1}$ at $0.95R_\odot$.

When comparing Fig. 2 to Fig. 6 and Fig. 4 to Fig. 4, it can be seen that increasing the flow amplitude u_0 from $20.0m.s^{-1}$ to $50.0m.s^{-1}$ doesn't change the radial and angular distribution of the flow; both profiles swarm around $0.86R_\odot, 0.76R_\odot$, respectively. The distinguishable difference in the amount of flow vectors is due to increased grid size increment to showcase what the written code can do with desired grid sizes. While the same increase in u_0 strengthens u_θ as can be seen when Fig. 1 to Fig. 5 and Fig. 4 to Fig. 7 are compared to one another. Once again the sharp change in directions are due to increased grid size increment to showcase what the written code can do with desired grid sizes.

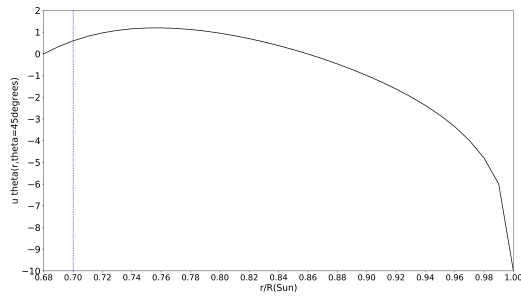


Fig. 1. Radial dependence of $u_\theta(r, \theta = 45^\circ)$ in Meridional Circulation Profile of Dikpati and Charbonneau 99 in which $u_0 = 20 \text{ m.s}^{-1}$, when radial grid is chosen to be $0.01R_{\odot}$, angular grid is chosen to be 2.0° . Blue dashed line indicates the bottom of the convection zone $0.7R_{\odot}$.

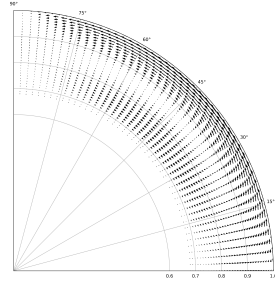


Fig. 2. Radial and angular flow distribution amongst the northern hemisphere of the Sun in Meridional Circulation Profile of Dikpati and Charbonneau 99 in which $u_0 = 20 \text{ m.s}^{-1}$, when radial grid is chosen to be $0.01R_{\odot}$, angular grid is chosen to be 2.0° . 1.0 indicates R_{\odot} , 0° the equator and 90° the pole.

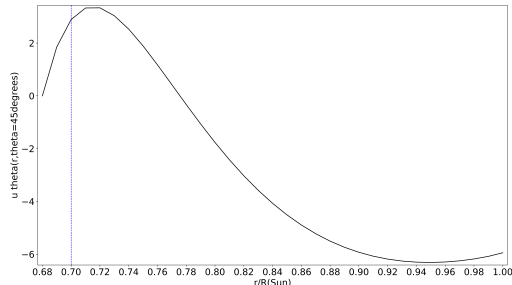


Fig. 3. Radial dependence of $u_\theta(r, \theta = 45^\circ)$ in Meridional Circulation Profile of Dikpati et.al 2004 in which $u_0 = 20 \text{ m.s}^{-1}$, when radial grid is chosen to be $0.01R_{\odot}$, angular grid is chosen to be 2.0° . Blue dashed line indicates the bottom of the convection zone $0.7R_{\odot}$.

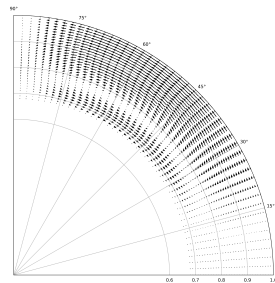


Fig. 4. Radial and angular flow distribution amongst the northern hemisphere of the Sun in Meridional Circulation Profile of Dikpati et.al 2004 in which $u_0 = 20 \text{ m.s}^{-1}$, when radial grid is chosen to be $0.01R_{\odot}$, angular grid is chosen to be 2.0° . 1.0 indicates R_{\odot} , 0° the equator and 90° the pole.

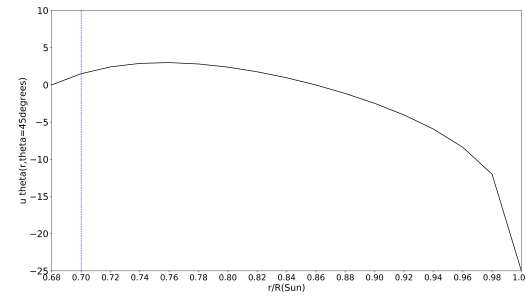


Fig. 5. Radial dependence of $u_\theta(r, \theta = 45^\circ)$ in Meridional Circulation Profile of Dikpati and Charbonneau 99 in which $u_0 = 50 \text{ m.s}^{-1}$, when radial grid is chosen to be $0.02R_{\odot}$, angular grid is chosen to be 5.0° . Blue dashed line indicates the bottom of the convection zone $0.7R_{\odot}$.

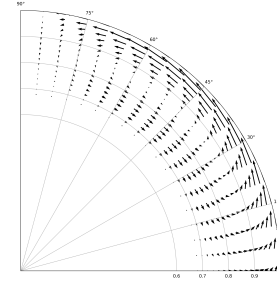


Fig. 6. Radial and angular flow distribution amongst the northern hemisphere of the Sun in Meridional Circulation Profile of Dikpati and Charbonneau 99 in which $u_0 = 50 \text{ m.s}^{-1}$, when radial grid is chosen to be $0.02R_{\odot}$, angular grid is chosen to be 5.0° . 1.0 indicates R_{\odot} , 0° the equator and 90° the pole.

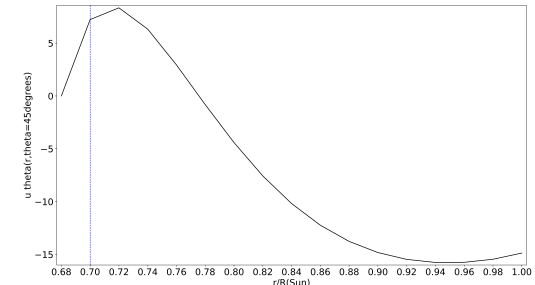


Fig. 7. Radial dependence of $u_\theta(r, \theta = 45^\circ)$ in Meridional Circulation Profile of Dikpati et.al 2004 in which $u_0 = 50 \text{ m.s}^{-1}$, when radial grid is chosen to be $0.02R_{\odot}$, angular grid is chosen to be 5.0° . Blue dashed line indicates the bottom of the convection zone $0.7R_{\odot}$.

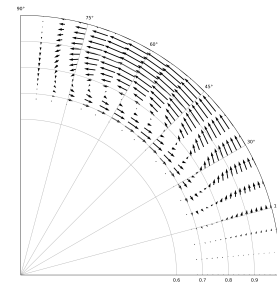


Fig. 8. Radial and angular flow distribution amongst the northern hemisphere of the Sun in Meridional Circulation Profile of Dikpati et.al 2004 in which $u_0 = 50 \text{ m.s}^{-1}$, when radial grid is chosen to be $0.02R_{\odot}$, angular grid is chosen to be 5.0° . 1.0 indicates R_{\odot} , 0° the equator and 90° the pole.

5. Conclusions

1. If a study dominated by the advective transport is more desired *profile1* would be more suitable since it spans the hemisphere more so than *profile2* does. *profile2* can be used for faster rotators, since they transport and accumulate more flux near the poles.(see Kővári & Oláh 2015; Reiners et al. 2014; Reinhold et al. 2014)
2. Radial and angular distribution of a profile doesn't change with varying u_0 but rather with m,p,q exponent values that dictate where the flow changes direction or gains strength. Varying u_0 changes maximum and minimum values of u_θ ; indicating that it can be manipulated accordingly.

Acknowledgements. I would like to thank E.Işık for his never ending support and T.Birkandan for an easy to comprehend introduction on Python 2.7.15 programming language. Please contact the author for the code used in this study.

References

- Babcock, H. W. 1961, The Astrophysical Journal, 133, 572
Dikpati, M. & Charbonneau, P. 1999, The Astrophysical Journal, 518, 508
Dikpati, M., de Toma, G., Gilman, P. A., Arge, C. N., & White, O. R. 2004, The Astrophysical Journal, 601, 1136
Hale, G. E. 1908, The astrophysical journal, 28, 315
Hale, G. E., Ellerman, F., Nicholson, S. B., & Joy, A. H. 1919, The Astrophysical Journal, 49, 153
Jiang, J., Cameron, R. H., Schmitt, D., & Işık, E. 2013, A&A, 553, A128
Jouve, L., Brun, A. S., Arlt, R., et al. 2008, A&A, 483, 949
Kővári, Z. & Oláh, K. 2015, Observing Dynamos in Cool Stars, Vol. 53, 457
Leighton, R. B. 1969, The Astrophysical Journal, 156, 1
Reiners, A., Schüssler, M., & Passegger, V. M. 2014, ApJ, 794, 144
Reinhold, T., Reiners, A., & Basri, G. 2014, in IAU Symposium, Vol. 302, Magnetic Fields throughout Stellar Evolution, ed. P. Petit, M. Jardine, & H. C. Spruit, 216–219
Schüssler, M. & Schmitt, D. 2004, A&A, 421, 349
Solanki, S. K., Inhester, B., & Schüssler, M. 2006, Reports on Progress in Physics, 69, 563